PIER C

(Received 15 February 2025, Accepted 1 April 2025, Scheduled 6 April 2025)

Investigation of Electromagnetic Interference Shielding Properties in PVDF-PVP Composite Films Reinforced with VGCNF

Harsh Mishra[1], Nikhil Negi[1], Vikas Rathi[1,*], Brijesh Prasad[2], and Varun Mishra[3]

[1]*Department of Electronics and Communication Engineering*
Graphic Era (Deemed to be University), Dehradun, Uttarakhand, India
[2]*Department of Mechanical Engineering*
Graphic Era (Deemed to be University), Dehradun, Uttarakhand, India
[3]*Department of Electronics Engineering*
Madhav Institute of Technology and Science, Gwalior, Madhya Pradesh, India

ABSTRACT: This paper presents a comparative study of electromagnetic interference (EMI) shielding properties of PVDF-PVP composite film with VGCNF as a conducting filler. The films were fabricated using solvent casting and further tested for their mechanical and thermal properties. The process was followed by a comparative analysis of shielding effectiveness calculated via dielectric parameters against the shielding measured through scattering parameters with the help of a network analyzer. Scanning Electron Microscopy was also done to better understand the morphological structure of the films. The film, with a thickness of around 0.18 mm, showcased shielding effectiveness within 25 dB–34 dB across a frequency band of 12 GHz to 18 GHz while being flexible and mechanically durable.

1. INTRODUCTION

In today's technology-driven world, a considerable boom is seen in the electronics field, which results from ever-increasing market demands. This begs the need for a way such that the seemingly infinite electronic components can work precisely without causing disturbances affecting each other. Any electromagnetic radiation from an electronic device that can compromise the intended working of any other device in its vicinity is termed EMI. It can result in system failures, inaccurate findings or even completely incorrect results [1, 2]. Yet, the market demand drives the shift towards higher frequency signals, which is accompanied by stronger effects of EMI, thus making the progress even more challenging. Not only this, but higher frequencies also pose serious threats towards our health, as shown in multiple case studies, to cause skin issues, cardiac irregularities, and migraines [3, 4].

To overcome these challenges associated with EMI, new strategies are being developed that emphasize efficiency, stability, and practical application. Conventional techniques, implementing metallic enclosures and electromagnetic filters, are effective but have notable limitations, such as added weight, bulkiness, and rigidity, which has prompted researchers and engineers to explore alternative solutions, with conductive polymer composites emerging as a promising innovation [5].

These conductive composites are created by the amalgamation of dielectric properties provided by the polymer part and the electrical conductivity of the filler counterpart. The produced conducting polymer composite replicates a net-like structure with numerous inter-connected routes that act as roadmaps for electrical charge. This principle of charge redistribution is responsible for effectively attenuating the impact of electromagnetic radiation via absorption and reflection. In this work, a thin and flexible film was fabricated in which EMI shielding through absorption was found to be dominant. Unlike shielding through reflection, it proves to be a better option for internal EMI suppression since it minimizes secondary interference. We analysed properties of the film not only from a result standpoint but also at a microscopic level to better our understanding regarding the actual working forces behind interference attenuation. This gave us a stronger fundamental foundation to work towards improvement in the said field.

Table 1 shows the comparative analysis of film thickness and its consequent shielding effectiveness of some of the preexisting films to our work. In our study, we used a solvent-casting procedure to fabricate our films. This is because, unlike in procedures such as melt blending, solvent casting allows for better dispersion of filler elements, preventing filler agglomeration while also being cost effective. We used a combination of polyvinylidene-fluoride (PVDF), which has a refractive index of ~ 1.43, and polyvinylpyrrolidone (PVP), which has a refractive index of ~ 1.52, to form our polymer matrix. PVP was used as an additive to slightly enhance the flexibility of the composite, while PVDF primarily provided thermal stability and dielectric strength [9]. Vapour Grown Carbon Nanofiber (VGCNF) was our pick for conductive filler. VGCNF is manufactured via the Chemical Vapour Deposition (CVD) method and provide multiple advantages as the conductive filler ele-

* Corresponding author: Vikas Rathi (vikas.rth@gmail.com).

TABLE 1. EMI shielding performance of other films.

Material used	Thickness (mm)	EMISE (dB)	Reference
LIG (Laser Induced Graphene)	0.05	10	[6]
pG (Pristine Graphene)	0.03	22.7	[7]
CH/Na (Sodium based chitosan)/CuSe	0.46	19.55	[8]
PVDF-PVP/VGCNF	0.18	30	This work

ment for this work. This was due to several pros including its high aspect ratio (length-to-diameter ratio $\sim$ 100–1000), leading to improved percolation of network channels, which helps in improving the overall conductivity of the film. Apart from having a high electrical conductivity of $\sim 10 \sim 4$ S/m, VGCNF remains thermally stable up to 600°C, all while improving the mechanical strength as well as flexibility of the film. Its fibrillar structure aids in uniform filler dispersion, and its lightweight nature improves practicality. An Ionic Liquid (IL) {1-Butyl-3-methylimidazolium hydrogen sulphate [BMIM][HSO4]} was used to provide a porous structure to the film which is essential for higher absorption of electromagnetic (EM) radiations [10, 11] while making the film lightweight [12, 13]. It is also characterized by low vapor production and high chemical stability with an abundance of ions [14], along with providing stronger chemical bonding ability [15]. IL along with DMF (N, N-Dimethylformamide) constituted the solvent portion for this composition. The general mechanism of EMI shielding is demonstrated in Fig. 1.

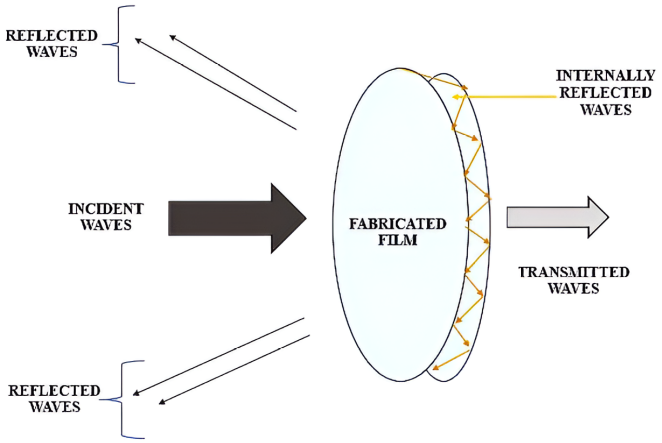

FIGURE 1. EMI shielding mechanism.

2. EXPERIMENTAL

2.1. Materials

The polymer composite films were formulated using PVDF (Poly(vinylidene fluoride)) and PVP (polyvinylpyrrolidone) as the polymer matrix, while ionic liquid (IL) and N, N-Dimethylformamide (DMF) served as the solvent mixtures. The materials were procured from Sigma-Aldrich. PVDF was utilized in its powdered form, exhibiting a density of 1.73 g/mol at ambient temperature (25°C), with a characterized molecular weight of 534,000 g/mol. The molecular weights of IL and PVP were recorded at 236.28 g/mol and 111.13 g/mol, respectively. For the conductive filler, Vapour Grown Carbon Nanofibers (VGCNFs) were employed, with DMF acting as the solvent.

2.2. Composite Film Fabrication

The initial preparation of the polymer matrix involved melting PVDF, followed by the incorporation of PVP as an additive to enhance conductivity and flexibility. Subsequently, VGCNF conductive filler was dry mixed with the polymer matrix using a magnetic stirrer for a duration of four hours at a speed of 600 rpm. This procedure is categorized under the pre-localization phase of the conducting term [16], which facilitates the coating of the conductive carbon nanofiber powder onto the polymer surface, thereby improving the spatial distribution homogeneity of the constituent particles. The dry mixture was then combined with ionic liquid (IL) and further dissolved in DMF. The resulting mixture was subjected to mixing at approximately 800 rpm until a homogeneous consistency was achieved. It was then placed in a glass petri dish, and the film was extracted after cooling, remaining undisturbed for 48 hours. The entire fabrication process is illustrated in Fig. 2. This procedure was repeated to fabricate 3 films in total, each with a different part-by-weight ratio of conductive filler VGCNF. Film F1 comprised 6 wt.%, film F2 11 wt.%, and film F3 1 wt.% of VGCNF, keeping the polymer matrix constant for all three. The concentration of VGCNF was decided through trial and error. A higher concentration of conductive filler does aid in enhancing shielding ability since overall conductivity increases, but it also decreases the film's mechanical strength and flexibility since filler dispersion becomes nonuniform. So, an acceptable trade-off between the two was found to be achieved using VGCNF concentration within 6 wt.% to 17 wt.%. The final thickness of the fabricated film was 0.18 mm.

2.3. Measurement of Shielding Effectiveness

2.3.1. Calculated Using Dielectric Parameters

The calculated shielding effectiveness (SE_C) was calculated using the dielectric parameters of the fabricated composites films. We used an impedance analyzer fixed along a test bench to determine the capacitance (C), dielectric constant (ε'), and dissipation factor ($\tan\delta$). For the test setup, counter-facing surfaces of subsequently placed samples were given a light coat of electrically conductive silver paint, and thin copper wires

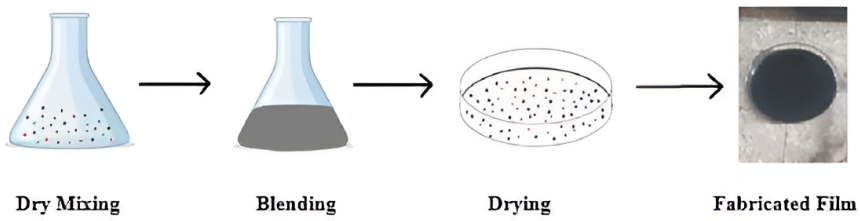

FIGURE 2. EMI shielding film fabrication.

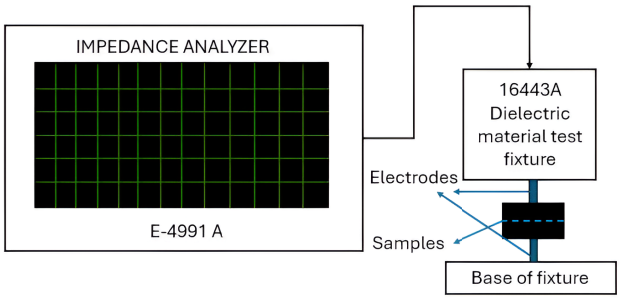

FIGURE 3. Dielectric measurement apparatus.

were then bonded to them. They were then targeted with an AC signal inside the test fixture whilst being placed between the electrodes. The overall setup is shown in Fig. 3.

The relative permittivity (ε') and AC conductivity (σ) were calculated using the formula:

$$\varepsilon' = Ct/\varepsilon_0 Ar \tag{1}$$

$$\sigma = \omega \cdot \varepsilon_0 \cdot \varepsilon' \tan\delta \tag{2}$$

where ε_0 is the permittivity of free space, Ar the area, t the thickness (0.18 mm), C the capacitance, and $\tan\delta$ the dissipation factor.

Furthermore, SE_C was evaluated as the sum of absorption and reflection losses along with the re-reflection correction factor. Absorption loss (A) was determined using:

$$A = 20\log 10e^{\frac{t}{\delta}} = 131t\sqrt{f\mu\sigma} \tag{3}$$

where μ is the magnetic permeability, and f is denotes the operational frequency. The reflection loss (R) was determined using:

$$R = 168 - 20\log_{10}\sqrt{\frac{f\mu}{\sigma}} \tag{4}$$

The re-reflection correction factor (C) was calculated by finding out the propagation constant (m) and reflection coefficient (Γ) and then implemented using the following relations:

$$m = 9.77 \times 10^{-10}\sqrt{\frac{f\mu}{\sigma}} \tag{5}$$

$$\Gamma = \frac{4 \times \left(1-m^2\right)^2 - 2m^2 + j2\sqrt{2m}\left(1-m\right)^2}{\left(\left(1+\sqrt{2m}\right)^2+1\right)^2} \tag{6}$$

$$C = 20\log\left[1 - \Gamma 10^{-\frac{A}{10}}\left(\cos 0.23A - j\sin 0.23A\right)\right] \tag{7}$$

2.3.2. Measurement Using Scattering Parameters

The practical assessment of film's shielding ability was conducted utilizing the method involving waveguide transmission [17]. In this approach, the composites were securely positioned within a segment of the waveguide, followed by the measurement of the scattering parameters at the two ports using a microwave network analyzer. Specifically, the fabricated sheets were secured within the Ku band waveguide adapter between the ports and linked to the microwave network analyzer (PNA, N5223A, Keysight), as illustrated in Fig. 4. This adapter acts as a controlled transmission line for the microwave. Such a waveguide transmission setup provides higher precision in the measurement of shielding effectiveness since it eliminates edge diffraction effects.

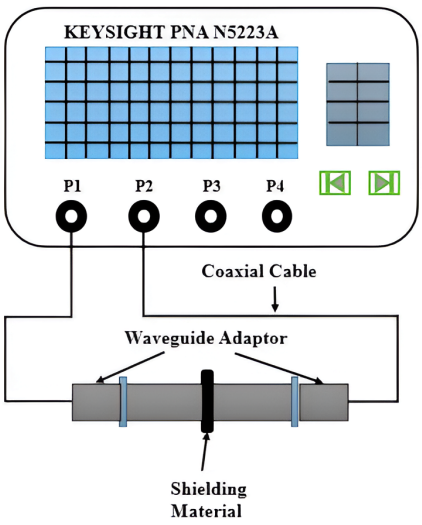

FIGURE 4. Shielding measurement apparatus.

The PNA Keysight analyzer was adjusted to correction, and the S-parameters S_{11} (corresponding to reflection) and S_{21} (corresponding to transmission) were recorded. The overall material EMI shielding effectiveness (SE_M) can be described as the degree of decrement in the intensity of incoming electromagnetic radiation after passing through the composite sheet. This can be calculated using the formula:

$$SE_M = 10\log\left(\frac{Pin}{Pout}\right) \tag{8}$$

Here, Pin and $Pout$ correspond to the incoming and outgoing powers from the fabricated sheet. Additionally, SE_M can

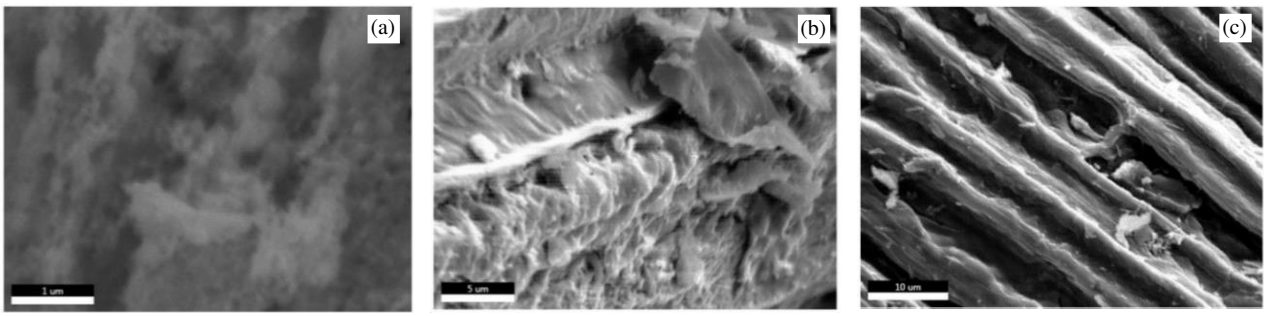

FIGURE 5. (a) SEM image of polymer matrix without VGCNF, (b) 11 wt.% VGCNF film's SEM image, (c) magnified image of the film with 17 wt.% VGCNF.

be understood as the summation of effective shielding through reflection (SE_R), absorption (SE_A), and multiple reflections (SE_{MM}). Therefore, SE_M can be further reformulated as

$$SE_M = SE_R + SE_A + SE_{MM} \tag{9}$$

Since SE_{MM} is comparatively very small, if SE_M exceeds 10 dB, we just neglect the multiple reflection counterpart meaning SE_M, then only depend on SE_R and SE_A. The reflection power (R), absorption power (A), and transmittance power (T) are interrelated by:

$$A + R + T = 1 \tag{10}$$

These factors are computed using:

$$R = |S_{11}|^2, \quad T = |S_{21}|^2 \tag{11}$$

Further, their contributing shielding efficiency through reflection and absorption are shown using the subsequent relations [18]:

$$SE_R = 10\log\left(\frac{1}{1-R}\right) = 10\log\left(\frac{1}{1-|S_{11}|^2}\right) \tag{12}$$

$$SE_A = 10\log\left(\frac{1-R}{T}\right) = 10\log\left(\frac{1-|S_{11}|^2}{|S_{12}|^2}\right) \tag{13}$$

3. RESULT ANALYSIS

3.1. Structural Analysis Discussion

Scanning Electron Microscopy (SEM) was done for the morphological analysis of the composites to get a deeper understanding of the film's structure. This helps understand the effects of crystalline layers in supporting the shielding effectiveness attribute of the polymer composite. Fig. 5(a) shows the imaging results of plain polymer matrix without any conductive filler. The lack of VGCNF is the reason behind the absence of any crystalline formations in the image. Fig. 5(b) showcases the SEM image for the complete film composition, comprising VGCNF by 11 wt.%. The presence of VGCNF filler results in the formation of ridges-like structures that act as pathways for charge distribution. This leads to the increase in the porous structure of film due to which the absorption phenomenon of film increases. In Fig. 5(c), we can see more defined channel formations and porosity due to a higher concentration of VGCNF with 17 wt.% film, facilitating an even better environment for charge dispersion.

3.2. Mechanical Strength Analysis

The produced composites were subjected to a tensile strength testing machine to test their load-sustaining abilities. This was done to verify the fabricated films' practical viability from a mechanical standpoint. The film with the least amount of conductive filler, i.e., F1 (6% VGCNF wt.) performed the best in this test as shown in Fig. 6. As the concentration of conductive filler increases, the composite becomes more brittle, hence we can observe that F3 (17 wt.% VGCNF film) shows the worst performance under stress out of the three.

3.3. Dielectric Analysis

As discussed in Section 2.3.1, the dielectric properties (dielectric constant (ε') and dissipation factor ($\tan\delta$)) of the samples were used to calculate the absorption and reflection of the composite films [5]. Fig. 7 presents the resultant dielectric constant as a function of frequency for all three films. It is evident that ε' increases with the concentration of VGCNF, indicating that higher filler content enhances the material's permittivity. Among the three, F3 exhibits the highest dielectric constant, attributed to its greater VGCNF content, which facilitates the formation of a more extensive conductive network. As frequency increases, the dielectric constant gradually declines, primarily due to the diminishing polarization effects at higher frequencies. This behaviour suggests that F3 has the highest charge storage capacity, while F1, with the lowest VGCNF content, demonstrates the least ability to store charge.

3.4. Thermal Analysis

The differential scanning calorimetry (DSC) measurements were used to investigate the impact of temperature on the films. The variation in flow of heat with respect to varied temperatures corresponding to each PVDF-PVP/VGCNF/IL film is displayed in Fig. 8. A peak associated with the melting phase transition can be seen in the curve at the melting temperature (Tm). Pure PVDF has a Tm about 168°C. The obtained

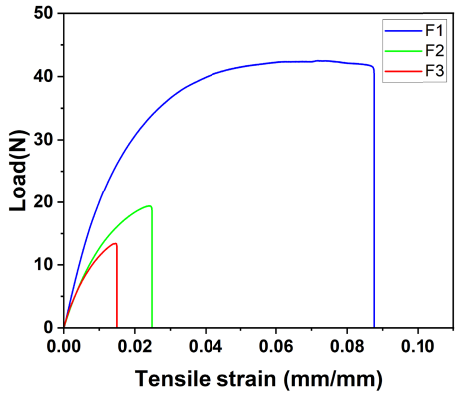

FIGURE 6. Load v/s strain curve for fabricated films with different concentrations of VGCNF.

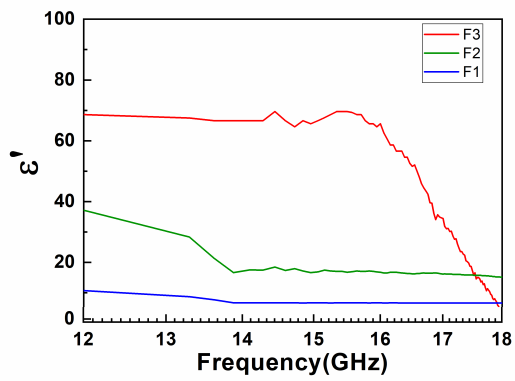

FIGURE 7. Dielectric constant for fabricated films F1, F2 and F3.

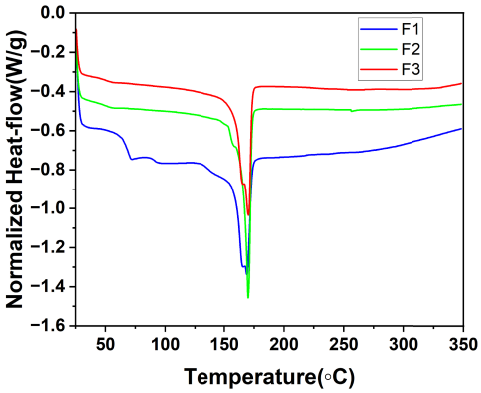

FIGURE 8. Thermal analysis.

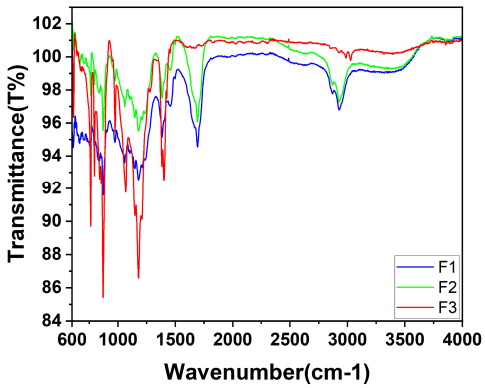

FIGURE 9. Transmittance v/s wavenumber curve for fabricated films F1, F2 and F3.

graph clearly shows that Tm stays almost constant even with the perforation of VGCNF and ionic liquid within the PVDF polymer matrix, indicating that the crystalline structure of the PVDF/VGCNF/IL composite sheet does not alter with changing temperature. The endothermic dip observed at $\sim$ 170°C–175°C signifies that the films start absorbing heat for thermal transition. Film F3(17 wt.% VGCNF) showcased the lowest dip, hence being the most thermally stable out of the three. The correction in dip upon further increments in temperature shows that the films stop absorbing excess heat for further transition. The normalized enthalpies of the melting transitions are unaffected by VGCNF and IL, even though they interact with the matrix. Hence, the overall crystalline structure is maintained throughout the varied concentrations of VGCNF.

3.5. FTIR Analysis

The Fourier-transform infrared (FTIR) spectra of the polymer composites illustrate distinct transmittance patterns, reflecting variations in chemical composition and polymer-filler interactions. Fig. 9 displays smoother characteristics for film F1 with fewer significant absorption peaks, indicating limited functional group activity or lower filler content, which is true since it is the results for 6 wt.% VGCNF film. In contrast, 11 wt.% VGCNF film (F2) presents more pronounced absorption bands in the mid-IR region ($\sim$ 1000–2000 cm^2), suggesting enhanced chemical interactions or the presence of additional functional groups. Finally, 17 wt.% VGCNF film (F3) shows deeper and more numerous absorption peaks, particularly in the initial region ($\sim$ 600–1500 cm^2), highlighting higher filler concentration or increased chemical complexity. The increase in spectral distortion is primarily due to higher infrared absorption and scattering from VGCNF. That is why the losses in spectra are seen most prominently in film F3 since it has the highest concentration of VGCNF. These differences in absorption intensity and peak distribution underline the influence of polymer-filler interactions and functionalization on the material's properties, which are crucial for optimizing EMI shielding performance.

3.6. Shielding Effectiveness Analysis

The shielding effectiveness via reflection and absorption is showcased in Fig. 10(a) and Fig. 10(b), respectively. The figures demonstrate that shielding ability through absorption (SE_A) is significantly higher than that through reflection (SE_R). F3 showed the highest SE_A within the range of 16 dB–24 dB, with its SE_R being the least within 5 dB–8 dB. It is clear from both the figures that as the concentration of VGCNF increases the absorption increases, and reflection decreases. This is due to the porous structure allowing deeper

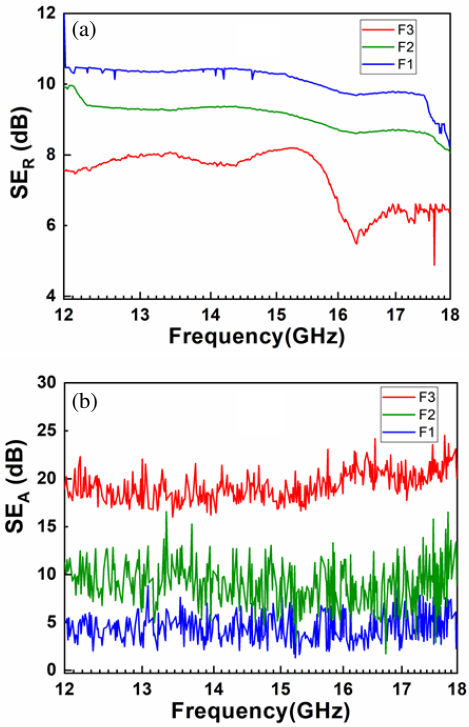

FIGURE 10. Shielding effectiveness v/s frequency curve (a) SE_R due to reflection, (b) SE_A due to absorption.

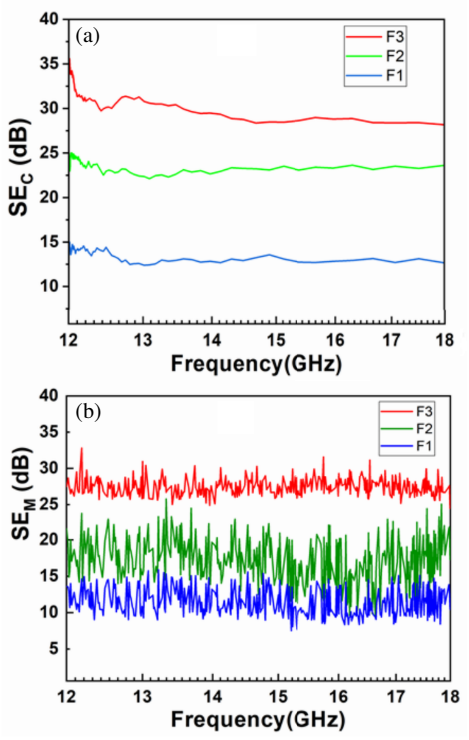

FIGURE 11. Shielding effectiveness v/s frequency curve (a) SE_C via dielectric properties, (b) obtained SE via scattering parameters.

penetration of incident waves, which are then dissipated through absorption. Thus, reflection is minimal, and hence, the mechanism of absorption acts as the primary source of shielding.

Fig. 11 shows a comparative study of (a) the total calculated shielding effectiveness obtained via dielectric properties alongside (b) the total obtained shielding effectiveness via scattering parameter measurements. The result lies in accordance with the theory, higher SE for higher concentrations of conductive filler. In Fig. 11(a), we can observe the SE_C value for 17 wt.% VGCNF film (F3) to be the highest out of the three, within a range of 34 dB to 27 dB across 12 GHz to 18 GHz frequency range. This is verified by Fig. 11(b), where the SE value for the same lies within a range of 33 dB to 25 dB. This trend seems to hold true for all three films. Thus, it is clear from the figures that SE_C lies in the proximity of SE_M obtained through scattering parameters.

4. CONCLUSION

In this work, the finally produced inexpensive composite films are both lightweight and flexible, along with decent shielding capabilities with absorption as key parameter. Film F1 showcased the strongest mechanical properties, while F3 provided the highest SE values. We can conclude that film F2 shows the most satisfactory result as it shows satisfactory SE value with both mechanisms, and it is mechanically durable. The composite film's flexible nature allows it to be applied to any electronic device, effectively reducing the impact of EMI.

REFERENCES

[1] Kong, L. B., Z. W. Li, L. Liu, R. Huang, M. Abshinova, Z. H. Yang, C. B. Tang, P. K. Tan, C. R. Deng, and S. Matitsine, "Recent progress in some composite materials and structures for specific electromagnetic applications," *International Materials Reviews*, Vol. 58, No. 4, 203–259, 2013.

[2] Geetha, S., K. K. S. Kumar, C. R. K. Rao, M. Vijayan, and D. C. Trivedi, "EMI shielding: Methods and materials — A review," *Journal of Applied Polymer Science*, Vol. 112, No. 4, 2073–2086, 2009.

[3] Morgan, D., *Handbook of EMC Testing and Measurement*, Institution of Electrical Engineers (IEE), London, 1995.

[4] Kheifets, L., A. A. Afifi, and R. Shimkhada, "Public health impact of extremely low-frequency electromagnetic fields," *Environmental Health Perspectives*, Vol. 114, No. 10, 1532–1537, 2006.

[5] Rathi, V., V. Panwar, G. Anoop, M. Chaturvedi, K. Sharma, and B. Prasad, "Flexible, thin composite film to enhance the electromagnetic compatibility of biomedical electronic devices," *IEEE Transactions on Electromagnetic Compatibility*, Vol. 61, No. 4, 1033–1041, 2018.

[6] Shahnawaz, M., H. B. Baskey, and M. J. Akhtar, "Ultra-thin LIG film for X band EMI shielding applications," in *2023 IEEE Microwaves, Antennas, and Propagation Conference (MAPCON)*, 1–4, Ahmedabad, India, 2023.

[7] Gupta, K., M. J. Nine, C. Denton, and D. Losic, "Electromagnetic shielding using graphene material in wide bandwidth of 1.5 GHz–10 GHz," in *2022 International Symposium on Antennas and Propagation (ISAP)*, 553–554, Sydney, Australia, 2022.

[8] Mazu, N. N., M. A. H. M. A. Majid, N. H. Osman, J. Y. C. Liew, and M. M. Ramli, "Shielding efficiency study of sodium based chitosan polymer with different types of filler," in *2020 IEEE International RF and Microwave Conference (RFM)*, 1–4, Kuala

Lumpur, Malaysia, 2020.

[9] Gargama, H., A. K. Thakur, and S. K. Chaturvedi, "Polyvinylidene fluoride/nanocrystalline iron composite materials for EMI shielding and absorption applications," *Journal of Alloys and Compounds*, Vol. 654, 209–215, Jan. 2016.

[10] Sampath, U. G. T. M., Y. C. Ching, C. H. Chuah, J. J. Sabariah, and P.-C. Lin, "Fabrication of porous materials from natural/synthetic biopolymers and their composites," *Materials*, Vol. 9, No. 12, 991, Dec. 2016.

[11] González, M., M. Crespo, J. Baselga, and J. Pozuelo, "Carbon nanotube scaffolds with controlled porosity as electromagnetic absorbing materials in the gigahertz range," *Nanoscale*, Vol. 8, No. 20, 10 724–10 730, 2016.

[12] Kocifaj, M., J. Klačka, F. Kundracik, and G. Videen, "Charge-induced electromagnetic resonances in nanoparticles," *Annalen der Physik*, Vol. 527, No. 11-12, 765–769, Dec. 2015.

[13] Kuang, T., L. Chang, F. Chen, Y. Sheng, D. Fu, and X. Peng, "Facile preparation of lightweight high-strength biodegradable polymer/multi-walled carbon nanotubes nanocomposite foams for electromagnetic interference shielding," *Carbon*, Vol. 105, 305–313, 2016.

[14] Plaquevent, J.-C., J. Levillain, F. Guillen, C. Malhiac, and A.-C. Gaumont, "Ionic liquids: New targets and media for α-amino acid and peptide chemistry," *Chemical Reviews*, Vol. 108, No. 12, 5035–5060, 2008.

[15] Lins, L. C., S. Livi, M. Maréchal, J. Duchet-Rumeau, and J.-F. Gérard, "Structural dependence of cations and anions to building the polar phase of PVDF," *European Polymer Journal*, Vol. 107, 236–248, Oct. 2018.

[16] Panwar, V., B. Kang, J.-O. Park, S. Park, and R. M. Mehra, "Study of dielectric properties of styrene-acrylonitrile graphite sheets composites in low and high frequency region," *European Polymer Journal*, Vol. 45, No. 6, 1777–1784, 2009.

[17] Nanni, F., P. Travaglia, and M. Valentini, "Effect of carbon nanofibres dispersion on the microwave absorbing properties of CNF/epoxy composites," *Composites Science and Technology*, Vol. 69, No. 3–4, 485–490, 2009.

[18] Bera, R., S. Paria, S. K. Karan, A. K. Das, A. Maitra, and B. B. Khatua, "NaCl leached sustainable porous flexible Fe_3O_4 decorated RGO-polyaniline/PVDF composite for durable application against electromagnetic pollution," *EXPRESS Polymer Letters*, Vol. 11, No. 5, 419–433, May 2017.